Editors' Choice

ORIGINAL PAPER

Nagoya J. Med. Sci. **85**. 528–541, 2023
doi:10.18999/nagjms.85.3.528

Supernatant from activated omentum accelerates wound healing in diabetic mice wound model

Yu Li, Kazunobu Hashikawa, Katsumi Ebisawa, Miki Kambe, Shinichi Higuchi and Yuzuru Kamei

Department of Plastic and Reconstructive Surgery, Nagoya University Graduate School of Medicine, Nagoya, Japan

ABSTRACT

Diabetic wounds are considered one of the most frequent and severe complications of diabetes mellitus. Recently, the omentum has been used in diabetic wound healing because of its tissue repair properties. The activated omentum is richer in growth factors than the inactivated, thereby contributing to the wound healing process. To further investigate the effect of activated omentum conditioned medium (aOCM) on diabetic wound healing, we injected supernatant from aOCM, saline-OCM (sOCM), inactivated-OCM (iOCM), and medium (M) subcutaneously upon creation of a cutaneous wound healing model in diabetic mice. Wound area (%) was evaluated on days 0, 3, 5, 7, 9, 11, 14, 21, and 28 post-operation. At 9 and 28 d post-operation, skin tissue was harvested and assessed for gross observation, neovascularization, peripheral nerve fiber regeneration, and collagen deposition. We observed that aOCM enhanced the wound repair process, with significant acceleration of epidermal and collagen deposition in the surgical lesion on day 9. Additionally, aOCM displayed marked efficiency in neovascularization and peripheral nerve regeneration during wound healing. Thus, aOCM administration exerts a positive influence on the diabetic mouse model, which can be employed as a new therapy for diabetic wounds.

Keywords: activated omentum, diabetic mellitus, diabetic wounds, wound healing, collagen

Abbreviations:
DWs: diabetic wounds
aOCM: activated omentum conditioned medium
sOCM: saline omentum conditioned medium
iOCM: inactivated omentum conditioned medium
WA: wound area

Received: July 6, 2022; accepted: October 4, 2022
Corresponding Author: Katsumi Ebisawa, MD, PhD
Department of Plastic and Reconstructive Surgery, Nagoya University Graduate School of Medicine, 65 Tsurumai-cho, Showa-ku, Nagoya 466-8550, Japan
Tel: +81-52-744-2525, E-mail: ebisawa@med.nagoya-u.ac.jp

INTRODUCTION

Global diagnostic criteria for diabetes mellitus has been harmonized by the World Health Organization, 8th edition of the International Diabetes Federation, and the American Diabetes Association,[1-3] According to these criteria, the current global diabetes prevalence is 8.8%, with a further increase expected to be 9.9% by the year 2045.[4] An increasing number of diabetes cases and their complications have caused a heavy health and economic burden for patients and their families. Furthermore, diabetic wounds (DWs) are the most common complications in patients with diabetes mellitus, which is a result of poor glycemic control, narrowed peripheral vessels, underlying neuropathy, and poor immune response.[5] Thus far, the available therapeutic approaches include good glycemic control, wound management, and surgical operation, but all of them have limitations and none appear adequate to guarantee successful, conclusive, non-recurrent healing. Hence, there is an urgent need for a therapeutic alternative to currently available treatments.

The omentum is a highly vascularized fibrous fatty layer of tissue located in the abdominal cavity, serving as a layer of coverage and protection. It is known to possess healing potential for over 100 years, mediated by omentum transportation, owing to its angiogenic, immunogenic, and lymphatic properties.[6-8] Goldsmith et al reported that omental transposition enhanced the healing and regeneration of neurons across a transected spinal cord in animal (cat) experiments and in one patient.[9-11] Omental scaffolds or omentum-derived vascular fractions has been demonstrated to promote peripheral nerve regeneration.[12-14] Additionally, patients who underwent reconstructive surgery related to the omentum-free flap showed improved peripheral nerve regeneration compared with other free flaps (in press). Further, it has been reported that the omentum can be activated in the presence of foreign bodied. Once activated, the flimsy sheet-like omentum not only increases in size and mass, but is also rich in growth factors,[15-17] thus, prin oviding important clues regarding the activation and application of the omentum in regenerative medicine. However, the components of the activated omentum and their effects on diabetic wound healing have not been investigated. The objective of this study was to investigate the exosomal protein groups that contribute to wound healing in activated omentum conditioned medium (aOCM) by mass spectrometry and to evaluate the effectiveness of aOCM on DWs using a diabetic mouse wound model.

MATERIALS AND METHODS

Animal

Animals received care in compliance with Nagoya University Guidelines for Animal Care and Use, which are based on the US National Research Council's criteria outlined in the Guide for the Care and the Use of Laboratory Animals. Sixteen female C57BL/6J mice (8-week-old) and 36 male genetically diabetic C57BLKS/J-*Lepr*^{db} (db/db) mice (12-week-old) were obtained from Japan SLC (Hamamatsu, Japan). After 1 week of adaptation, the diabetic mice were housed individually. All animals had free access to standard food and water, and were housed in an animal care facility maintained on a 12-h light/dark cycle at 24 °C.

Preparation of activated omentum conditioned medium

Activation of omentum by foreign bodies. C57BL/6 male mice (20–25 g) were randomly divided into three groups: (1) the control group (c), which served as a negative control without any interference (n = 6); (2) the saline group (s), where 0.5 mL saline was injected intraperitoneally (n = 5); and (3) the activated group (a), where 0.5 mL polydextran particle slurry

(Biogel P-60, 120 μM; Biorad Laboratories, Richmond Calif; 1:1 in normal saline) was injected intraperitoneally[16] (n = 5). After 2 weeks, the animals were laparotomized, and the omentum was harvested and processed as described further.

Collection of the supernatant. The harvested omentums were immediately washed using sterile ice-cold phosphate-buffered saline (PBS) three times. Further, the omentums were immersed in 6-well plates (1 per well) in Dulbecco's Modified Eagle Medium/Nutrient Mixture F-12, 10% fetal bovine serum, and 1% antibiotic/antimycotic solution (100 μg/mL penicillin and 100 μg/mL streptomycin; Wako) and cultured in an atmosphere of 5% CO_2 at 37 °C. The supernatant was collected after 48 h of culture and centrifuged at 15000 rmp for 10 min at 4 °C two times. Additionally, a serum-free medium was used for mass spectrometry analysis. Protein content was measured using the Bradford protein concentration assay after supernatant collection.[18] To avoid degradation, the supernatant was stored at –78 °C. The supernatants collected from the (c), (s), and (a) groups were named inactivated omentum conditioned medium (iOCM), saline omentum conditioned medium (sOCM), and activated omentum conditioned medium (aOCM), respectively.

Diabetic mice wound model

An excisional wound-splinting model was generated as described previously.[19] Briefly, C57BLKS/J *Lepr*^{db} (db/db) mice were anesthetized using isoflurane gas (3% induction, 2% maintenance) and the hair on the dorsal skin was removed. Two 8 × 8 mm full-thickness circular wounds were created bilaterally on the dorsal thoracic spine. A donut-shaped silicone ring (Shinoda Gomu Co Ltd, Tokyo, Japan) with an 8-mm inner diameter was placed around the wound and fixed in place. The ring was then sutured around the wound using six 4-0 nylon sutures (Fig. 1A). Postoperative mice were randomly assigned to four groups, which were treated with medium (M) (n = 6), iOCM (n = 6), sOCM (n = 12), and aOCM (n = 12). The supernatant (250 μL) was injected into 4 sites at the edge of wounds and center of the wound beds evenly (Fig. 1B). All mice were treated with a Tegaderm dressing (3M, MN, USA) to cover the wounds.

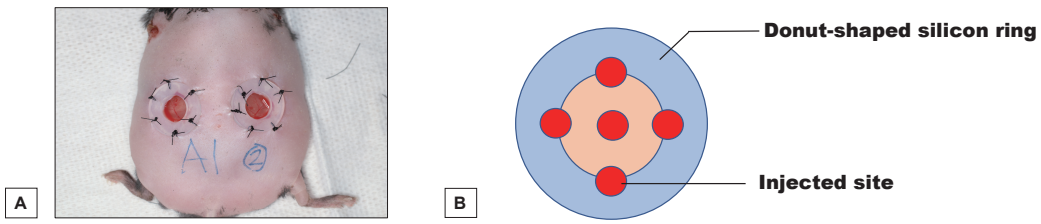

Fig. 1 Description of operation and administration

Fig. 1A: Diabetic mice wound model – two 8 × 8 mm full-thickness circular wounds were created bilaterally on the dorsal thoracic spine. A donut-shaped silicone ring with an 8-mm inner diameter was placed around the wound and fixed in place. The ring was sutured around the wound using six 4-0 nylon sutures.

Fig. 1B: Conditioned media administration – the supernatant (250 μL) was injected at four sites at the edge of wounds and at the center of the wound beds evenly (50 μL per point).

Wound closure analysis

Each wound site was photographed using a digital camera (Canon Inc, Tokyo, Japan) on days 0, 3, 5, 7, 9, 11, 14, 21, 28 post-operation and wound areas were analyzed using ImageJ analysis software (Image J, Bethesda, Maryland, USA). The percentage of wound closure (WC%) was calculated as follows: WC% = WA_T/WA_0 (WA_T, wound area at each time point; WA_0, wound area at day 0). The days to first of 50% healing were recorded for every wound and the average

of 50% healing days were calculated.

Histological Analyses

Skin tissue around surgical defects was harvested at 9- and 28-days post-operation and fixed in 4% paraformaldehyde, paraffin-embedded, and 4 μm paraffin sections were prepared, followed by hematoxylin and eosin (H&E) staining for gross observation. Collagen fibers were assessed using Masson's trichrome staining, and three randomly selected fields from each specimen (n = 3/group) were imaged using light microscopy (Olympus Tokyo, Japan). The collagen volume fraction (CVF) of each sample was evaluated using image J software as previously described[20] for assessment of full recovery of the impaired skin tissue.

Immunofluorescence staining

Skin sections, 9- days post-operation, were immunostained with anti-alpha-smooth muscle actin (α-SMA) antibody (1:300 dilution, Proteintech, USA) and CD31 (1:20 dilution, Dianova, Hamburg Germany) to evaluate neo-vascularization and with neurofilament (NF-L) antibody (1:300 dilution, Proteintech USA) to assess the degree of nerve regeneration degree induced by the aOCM in the wounded skin. Incubation was done overnight at 4 °C. To enable fluorescence detection, sections were incubated with Alexa Fluor 555-labeled goat anti-rabbit IgG (1:500 dilution, Cell Signaling) and 488-labeled goat anti-rat IgG (1:500 dilution, Cell Signaling) secondary antibody at 25 °C for 40 min. The nuclei were stained with 4′,6-diamidino-2-phenylindole (DAPI, Southern Biotech). Stained tissue sections were imaged using a light microscope (Olympus, Tokyo, Japan). We randomly selected two areas at two sides of wound under 200x and 400x magnification at the edge of the wounds on day 9 post-operation as previously described[21] to count vessel and nerve fiber numbers respectively. All quantification experiments were performed by a blinded investigator.

Statistical analyses

All statistical analyses were performed using GraphPad Prism 6.0 for Windows (GraphPad Software, San Diego, CA, USA, www.graphpad.com). Data are reported as mean ± standard deviation (SD) and were analyzed using one-way analysis of variance (ANOVA). The differences were considered significant at $p < 0.05$.

RESULTS

Characteristics of activated omentum and aOCM

The intraperitoneal injection of polydextran particles caused the omentum to spread rapidly and was activated within 2 weeks (Fig. 2A). Notably, the omentum of group (a) gained significantly more weight than that of groups (c) and (s) (Fig. 2B). To investigate the protein abundance in the supernatant, we measured the protein content. In the iOCM, sOCM, and aOCM groups, the protein concentration was 1.059 ± 0.1097, 1.172 ± 0.074, and 2.602 ± 0.8177 (μg/μL), respectively, with group (a) having significantly higher protein than that in the (c) and (s) groups ($p < 0.05$) (Fig. 2C).

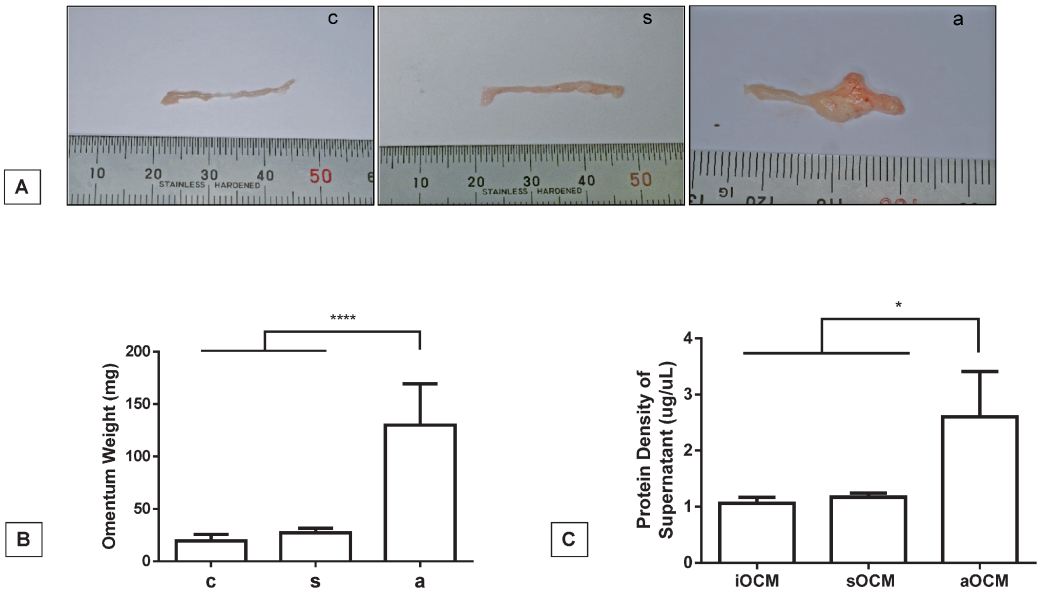

Fig. 2 Characteristics of activated omentum and aOCM

Fig. 2A: Representative images of harvested omentum from control (c), saline-injected (s), polydextran particle-injected (a) groups.

Fig. 2B: Omentum weight in each group. ****$p < 0.0001$.

Fig. 2C: Protein concentration in each group. *$p < 0.05$. Results are represented as mean ± standard deviation (SD).

iOCM: inactivated omentum conditioned medium

sOCM: saline omentum conditioned medium

aOCM: activated omentum conditioned medium

aOCM accelerated re-epithelialization in a diabetic murine wound model

To investigate whether aOCM could promote wound repair, we evaluated wound healing rates after M, iOCM, sOCM, and aOCM treatment. Wound areas diminished in a time-dependent manner in all treated groups, as shown in the time-course images (Fig. 3A). According to wound closure analysis, the aOCM group showed smaller WC% than that in the other three groups, thus demonstrating that aOCM significantly accelerated wound closure from day 7 to day 11 compared to that in the M, iOCM, and sOCM groups (Fig. 3B). The rate of wound healing was significant at around day 9 post-operation, hence we performed histological analysis on day 9 after operation. Furthermore, the time taken for 50% wound healing was 8.13 ± 0.99, 8.83± 1.47, 8.22 ± 1.35, 5.35 ± 0.79% days in the M, iOCM, sOCM, and aOCM groups, respectively, where healing time in aOCM was significantly faster than that in the other three groups ($p < 0.0001$) (Fig. 3C). However, time taken for complete wound healing for 4 groups was 17.88 ± 2.36, 18.00 ± 1.27, 19.28 ± 2.89, 16.76 ± 2.86 days, respectively (Fig. 3D), and no statistical difference was detected between four groups. H&E staining of the healed tissue at 9 and 28 days revealed gross wound processing. The four groups achieved complete wound healing at day 28, and on day 9, aOCM had a higher degree of re-epithelization than that in the M, iOCM, and sOCM groups (Fig. 3E), which is consistent with the wound closure analysis.

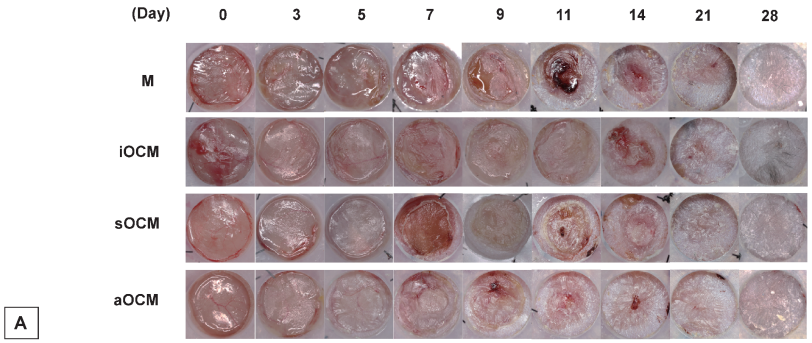
(Day)
0
3
5
7
9
11
14
21
28
M
iOCM
sOCM
aOCM

A

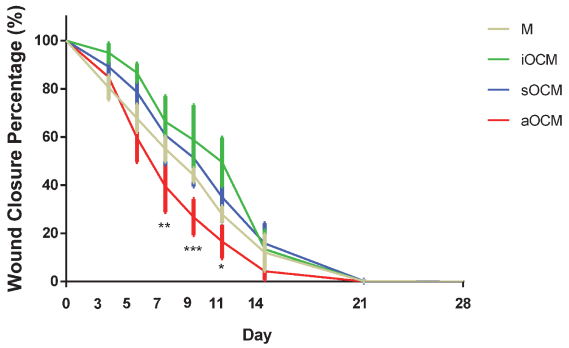
Wound Closure Percentage (%)
100
80
60
40
20
0
0 3 5 7 9 11 14 21 28
Day
**
***
*
M
iOCM
sOCM
aOCM

B

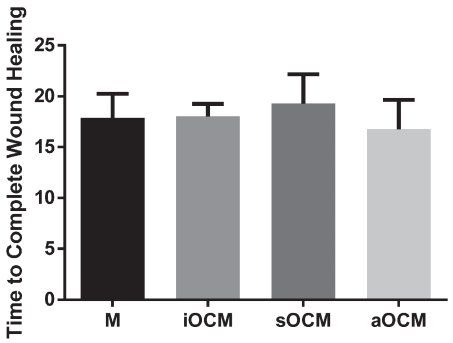
Time to Complete Wound Healing
25
20
15
10
5
0
M
iOCM
sOCM
aOCM

C

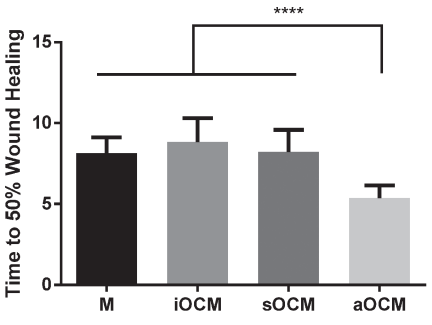
****
Time to 50% Wound Healing
15
10
5
0
M
iOCM
sOCM
aOCM

D

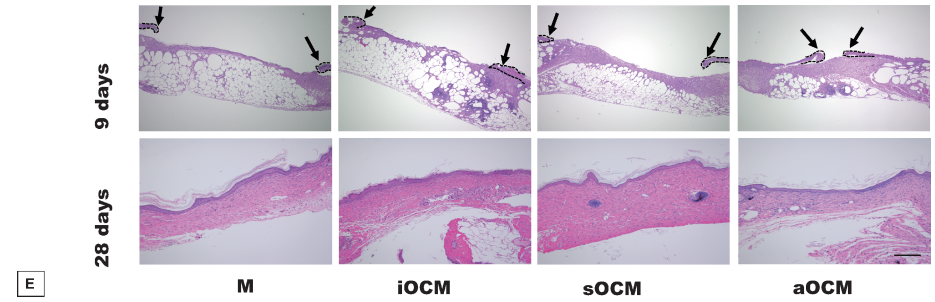

Fig. 3 Wound closure analysis of aOCM in diabetic mice wound model

Fig. 3A: Representative time-course images of wound closure on 8 mm biopsy punch excisional wound model after treatment with M, iOCM, sOCM, and aOCM.

Fig. 3B: The wound closure percentage (WC%) was determined on days 0, 3, 5, 7, 9, 11, 14, 21, 28 post-operation in each group. *$p < 0.05$; **$p < 0.01$; *** $p < 0.001$.

Fig. 3C: Average time taken for 50% wound healing in M, iOCM, sOCM, and aOCM groups. ****$p < 0.0001$.

Fig. 3D: Average time taken for complete wound healing in M, iOCM, sOCM, and aOCM groups.

Fig. 3E: Representative H&E-stained sections on day 9 and 28, as indicated, after treatment with M, iOCM, sOCM, and aOCM. The wound edges are indicated by red arrows. Scale bar = 500 μm. Results are represented as mean ± SD.

M: medium
iOCM: inactivated omentum conditioned medium
sOCM: saline omentum conditioned medium
aOCM: activated omentum conditioned medium

aOCM effects on angiogenesis and regeneration of peripheral nerve fibers

Angiogenesis is vital for wound healing due to the increased demand for nutrients and oxygen delivery to the wound bed. Peripheral nerve fibers are also important for the recovery of diabetic wounds. Newly formed vessels at the wound sites were examined by CD31 and α-SMA co-staining. As shown in Fig. 4A, the aOCM-treated group showed new blood vessel formation 9 days post-operation. The average vessel number in the aOCM group was significantly higher than other three groups ($p < 0.001$) (Fig. 4B). Additionally, newly formed peripheral nerve fibers were

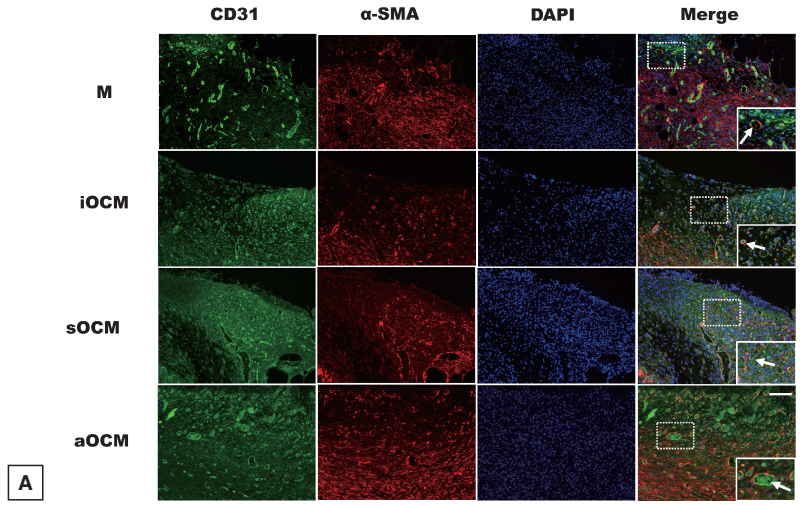

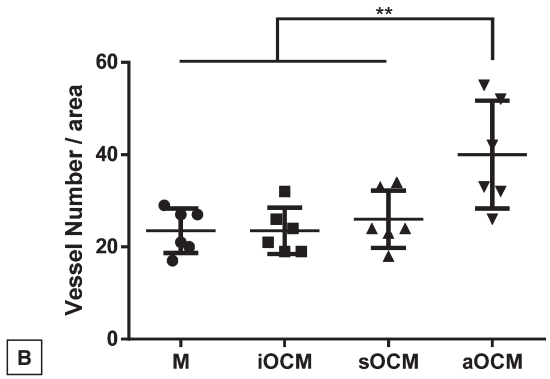
**
60
40
20
0
Vessel Number / area
M
iOCM
sOCM
aOCM

B

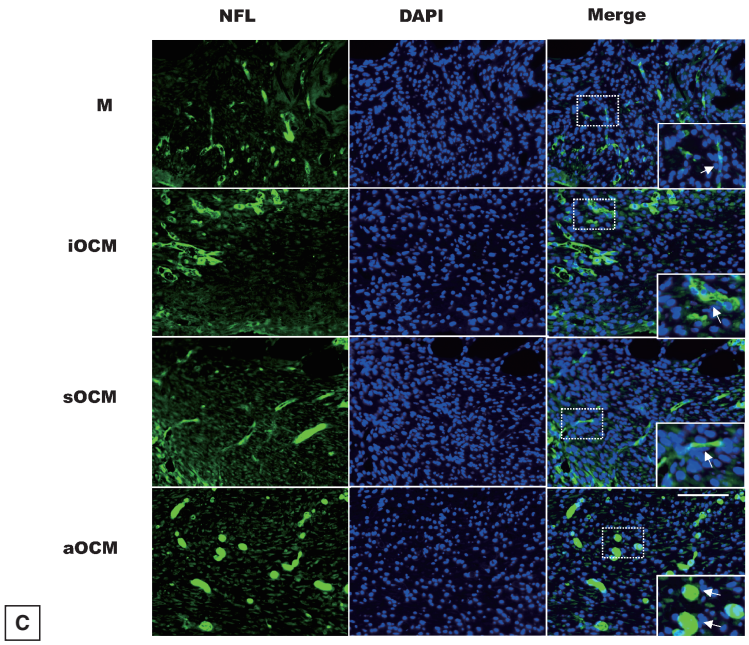
NFL
DAPI
Merge
M
iOCM
sOCM
aOCM

C

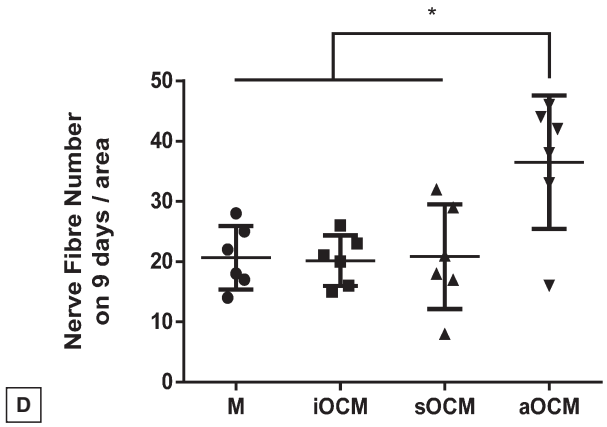

Fig. 4 Immunofluorescence assessment of angiogenesis and peripheral nerve fibers regeneration

Fig. 4A: Representative images of CD31 (green) and α-SMA (red) co-staining in the wound tissue on day 9 after treatment with M, iOCM, sOCM, and aOCM. Scale bar = 100 μm.

Fig. 4B: Quantitative analysis of angiogenesis assessed by CD31 and α-SMA co-staining. $^{**}p < 0.01$.

Fig. 4C: Representative images of NF-L staining (green) in the wound tissue on day 9 after treatment with M, iOCM, sOCM, and aOCM. Scale bar = 50 μm.

Fig. 4D: Quantitative analysis of peripheral nerve fiber stained by NF-L on day 9. $^{*}p < 0.05$. Results are represented as the mean ± SD. Nuclei were counterstained with DAPI (blue).

M: medium
iOCM: inactivated omentum conditioned medium
sOCM: saline omentum conditioned medium
aOCM: activated omentum conditioned medium

stained with NF-L antibody (Fig. 4C) and quantified in M, iOCM, sOCM, and aOCM groups at day 9 which were 20.67 ± 5.28, 20.17 ± 4.17, 20.83 ± 8.70, and 36.50 ± 11.0, respectively ($p < 0.05$) (Fig. 4D).

aOCM promoted collagen density in diabetic mice model

Collagen fibers are indispensable in the wound healing process because they provide strength and maintain structural integrity of the skin tissue, which is attributed to fibroblast proliferation, differentiation, and aggregation. Thus, collagen density is an important parameter in evaluating the histological state of wound healing. Masson's trichome staining was performed 9- and 28-days post-operation (Fig. 5A) to observe collagen density. aOCM administration significantly enhanced CVF as demonstrated by increased blue-stained, especially on day 9 post-operation. The CVF was 58.94 ± 8.84, 57.11 ± 5.65, 57.11 ± 5.65, and 73.25 ± 6.74% in M, iOCM, sOCM, and aOCM, respectively ($p < 0.0001$) (Fig. 5B). Additionally, after day 28 post-operation, the extent of collagen deposition was similar between the four groups (Fig. 5C).

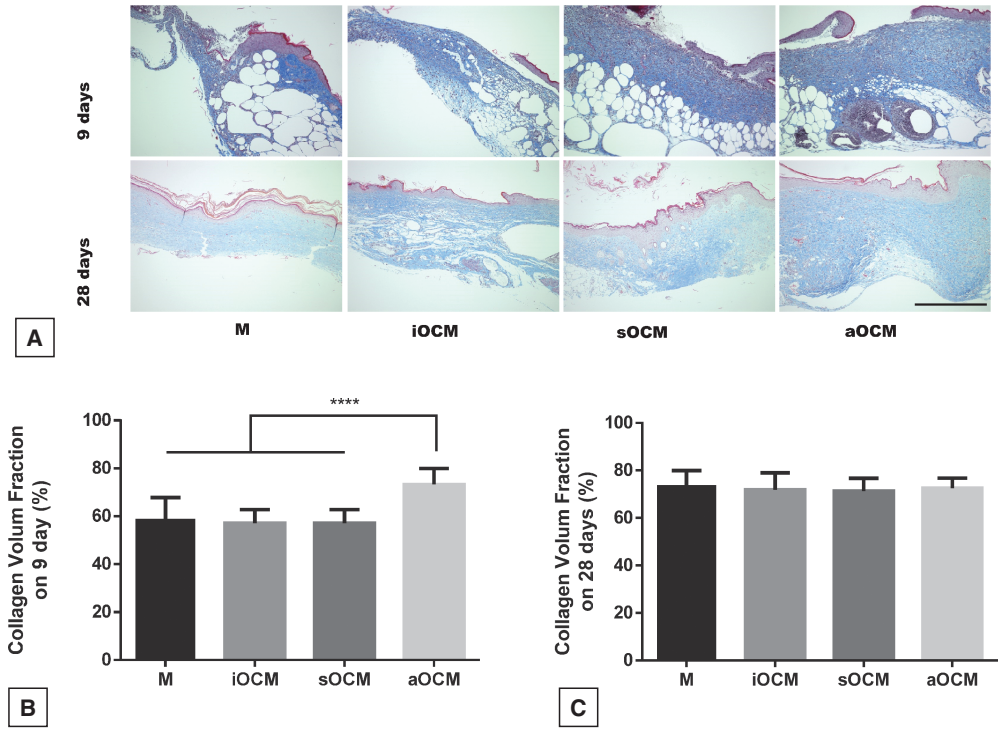

Fig. 5 Masson's trichome staining assessment of collagen deposition

Fig. 5A: Representative images of Masson's trichome staining of full-thickness excisional wounds in mice on day 9 and 28 after treatment with M, iOCM, sOCM, and aOCM. Collagen fibers are stained blue. Scale bar = 500 μm.

Fig. 5B: Collagen volume fraction (CVF) against stained section of each group was calculated through collagen-stained area (blue) relative to total stained area on day 9 post-operation. ****$p < 0.0001$.

Fig. 5C: CVF of each group on day 28 post-operation. Results are represented as mean ± SD.

M: medium
iOCM: inactivated omentum conditioned medium
sOCM: saline omentum conditioned medium
aOCM: activated omentum conditioned medium

DISCUSSION

Omentum has been used for diabetic wounds in the past decades because of its biological properties, including neovascularization, immunomodulatory activity, tissue healing and regeneration.[22] In clinics, the omentum-free flap has a wide variety of applications in reconstructive surgery and has been shown to be a reliable donor tissue.[23] Studies have indicated that the regenerative efficacy of the omentum is mediated by a potent paracrine mechanism involving molecules that contribute to tissue regeneration.[24,25] Further, it has been reported that activated omentum become a rich source for growth factors including fibroblast growth factor and vascular endothelial growth factor.[16,26] However, the effect of supernatant from aOCM on DWs has not been reported. Here, we demonstrate for the first time that aOCM can accelerate wound healing in diabetic mice.

DWs are induced by vascular insufficiency and peripheral nerve damage, therefore, therapy for vascular and nerve recovery is important for patients with diabetes mellitus. Transgenic diabetic mice have been reported to show properties similar to of patients with DWs.[27] In the

present study, animal experiments demonstrated that aOCM significantly accelerated the re-epithelialization rate from days 7 to 11 post-operation. In early wound healing process, aOCM tended to promote angiogenesis and peripheral nerve fibers regeneration at the edges of the wound. Moreover, our findings indicate that aOCM can promote collagen deposition in the early stages of wound healing in diabetic mice. Interestingly, the result of peripheral nerve regeneration degree treated with aOCM is different from our previous study, which used exosomes derived from induced pluripotent stem cells for skin regeneration.[21] Additionally, according to our mass spectrometry analysis, the aOCM group had abundant proteins, which potentially contributed to re-epithelialization, granulation tissue formation, inflammatory regulation, neovascularization, and peripheral nerve regeneration (Table 1).

Table1 Proteins potentially contributed to wound healing process

Accession	Description	MW [kDa]	PSM			Contribution to wound healing	Reference
			iOCM	sOCM	aOCM		
O70370	Cathepsin S	38.45	1	6	53	Angiogenesis; Wound closure	[28, 29, 30]
Q61292	Laminin subunit beta-2	196.45	2	8	62	Angiogenesis; Re-epithelization	[31]
Q91X72	Hemopexin	51.29	15	12	333	Enhanced peripheral nerve regeneration	[32, 33, 34]
P35441	Thrombospondin-1	129.56	6	17	67	Re-epithelization	[35]
Q61554	Fibrillin-1	312.08	30	68	259	Formation of granulation	[36, 37]
Q8VCM7	Fibrinogen gamma chain	49.36	12	17	98	Angiogenesis; Formation of granulation	[38, 39]
Q61001	Laminin subunit alpha-5	403.79	6	13	44	Re-epithelization; Collagen deposition	[40, 41]
P01027	Complement C3	186.37	54	64	394	Collagen deposition	[42]
P11276	Fibronectin	273.36	102	161	512	Re-epithelization, Collagen deposition; angiogenesis	[43, 44]
Q62009	Periostin	93.08	–	–	91	Collagen deposition	[45, 46]
P16110	Galectin-3	27.50	–	–	33	Angiogenesis; Peripheral nerve regeneration; Re-epithelization; Fibrous formation	[47, 48, 49]
O09049	Regenerating islet-derived protein 3-gamma	19.294	–	–	26	Peripheral nerve regeneration; Re-epithelization	[50, 51, 52]

iOCM: inactivated omentum conditioned medium
sOCM: saline omentum conditioned medium
aOCM: activated omentum conditioned medium
MW: molecular weight
PSM: peptide spectrum match

Although we did not clarify the detailed mechanisms of aOCM-induced effects, it is possible that the protein groups identified by mass spectrometry analysis contribute to wound healing. Moreover, several identified proteins are already being used as clinical therapeutics such as fibrillin-1,[53] fibronectin,[54] and laminin subunit beta-2Fu.[55] Nevertheless, further experiments are necessary to determine the molecular mechanisms underlying these observed effects. Additionally, despite the fact that the omentum is regarded as a reliable donor site in recent studies,[14,23,26,56] the donor-site morbidity and complications such as intestinal obstruction and herniation remain after omentum harvesting. Our study used conditioned medium from the activated omentum, which is abundant in groups of proteins and potentially contributes to wound healing in a diabetic mouse wound model. Our findings in animals support the potential use of aOCM for wound treatment in patients with diabetes. Taken together, the cocktail gel or mixture minimizes donor-site morbidity in the future and it may provide a new therapeutic method for treating DWs.

ACKNOWLEDGEMENTS

This study was supported by JSPS KAKENHI (grant number 16K11362). Y Li would like to thank the Otsuka Toshimi Scholarship Foundation for financial support (21–78). The authors wish to acknowledge the Division for Medical Research Engineering, Nagoya University Graduate School of Medicine, for technical support with mass spectrometry.

CONFLICTS OF INTEREST

The authors certify that no actual or potential conflicts of interest exist in relation to this article.

REFERENCES

1 American Diabeties Association. 2. Classification and diagnosis of diabetes: *Standards of Medical Care in Diabetes-2018*. *Diabetes care*. 2018;41(Suppl 1):S13-S27. doi:10.2337/dc18-S002.

2 World Health Organization. Definition and diagnosis of diabetes mellitus and intermediate hyperglycaemia: report of a WHO/IDF consultation. https://apps.who.int/iris/handle/10665/43588. Accessed April 21, 2006.

3 Patterson CC, Karuranga S, Salpea P, et al. Worldwide estimates of incidence, prevalence and mortality of type 1 diabetes in children and adolescents: Results from the International Diabetes Federation Diabetes Atlas, 9th edition. *Diabetes Res Clin Pract*. 2019;157:107842. doi:10.1016/j.diabres.2019.107842.

4 Standl E, Khunti K, Hansen TB, Schnell O. The global epidemics of diabetes in the 21st century: Current situation and perspectives. *Eur J Prev Cardiol*. 2019;26(2_suppl):7–14. doi:10.1177/2047487319881021.

5 Patel S, Srivastava S, Singh MR, Singh D. Mechanistic insight into diabetic wounds: Pathogenesis, molecular targets and treatment strategies to pace wound healing. *Biomed Pharmacother*. 2019;112:108615. doi:10.1016/j.biopha.2019.108615.

6 Bilgiç T, İnce Ü, Narter F. Autologous omentum transposition for regeneration of a renal injury model in rats. *Mil Med Res*. 2022;9(1):1. doi:10.1186/s40779-021-00361-0.

7 Krist LF, Eestermans IL, Steenbergen JJ, et al. Cellular composition of milky spots in the human greater omentum: an immunochemical and ultrastructural study. *Anat Rec*. 1995;241(2):163–174. doi:10.1002/ar.1092410204.

8 Zhang QX, Magovern CJ, Mack CA, Budenbender KT, Ko W, Rosengart TK. Vascular endothelial growth factor is the major angiogenic factor in omentum: mechanism of the omentum-mediated angiogenesis. *J Surg Res*. 1997;67(2):147–154. doi:10.1006/jsre.1996.4983.

9 Goldsmith HS, Brandt M, Waltz T. Near total transaction of human spinal cord: a functional return following omentum-collagen reconstruction. In: Goldsmith HS, ed. *The omentum: application to brain and spinal*

cord. Wilton: Forefront Publishing; 2000:76–92.
10 Goldsmith HS. The evolution of omentum transposition: from lymphedema to spinal cord, stroke and Alzheimer's disease. *Neurol Res*. 2004;26(5):586–593. doi:10.1179/016164104225017622.
11 Goldsmith HS, de la Torre JC. Axonal regeneration after spinal cord transection and reconstruction. *Brain Res*. 1992;589(2):217–224. doi:10.1016/0006-8993(92)91280-R.
12 Castañeda F, Kinne RK. Omental graft improves functional recovery of transected peripheral nerve. *Muscle Nerve*. 2002;26(4):527–532. doi:10.1002/mus.10229.
13 Mohammadi R, Azizi S, Delirezh N, Hobbenaghi R, Amini K. Transplantation of uncultured omental adipose-derived stromal vascular fraction improves sciatic nerve regeneration and functional recovery through inside-out vein graft in rats. *J Trauma Acute Care Surg*. 2012;72(2):390–396. doi:10.1097/TA.0b013e31821181dd.
14 Zhang YG, Huang JH, Hu XY, Sheng QS, Zhao W, Luo ZJ. Omentum-wrapped scaffold with longitudinally oriented micro-channels promotes axonal regeneration and motor functional recovery in rats. *PLoS One*. 2011;6(12):e29184. doi:10.1371/journal.pone.0029184.
15 García-Gómez I, Goldsmith HS, Angulo J, et al. Angiogenic capacity of human omental stem cells. *Neurol Res*. 2005;27(8):807–811. doi:10.1179/016164105X63674.
16 Litbarg NO, Gudehithlu KP, Sethupathi P, Arruda JA, Dunea G, Singh AK. Activated omentum becomes rich in factors that promote healing and tissue regeneration. *Cell Tissue Res*. 2007;328(3):487–497. doi:10.1007/s00441-006-0356-4.
17 Singh AK, Patel J, Litbarg NO, et al. Stromal cells cultured from omentum express pluripotent markers, produce high amounts of VEGF, and engraft to injured sites. *Cell Tissue Res*. 2008;332(1):81–88. doi:10.1007/s00441-007-0560-x.
18 Jones CG, Daniel Hare J, Compton SJ. Measuring plant protein with the Bradford assay: 1. Evaluation and standard method. *J Chem Ecol*. 1989;15(3):979–992. doi:10.1007/BF01015193.
19 Chen L, Mirza R, Kwon Y, DiPietro LA, Koh TJ. The murine excisional wound model: Contraction revisited. *Wound Repair Regen*. 2015;23(6):874–877. doi:10.1111/wrr.12338.
20 Yang YW, Zhang CN, Cao YJ, et al. Bidirectional regulation of i-type lysozyme on cutaneous wound healing. *Biomed Pharmacother*. 2020;131:110700. doi:10.1016/j.biopha.2020.110700.
21 Kobayashi H, Ebisawa K, Kambe M, et al. Effects of exosomes derived from the induced pluripotent stem cells on skin wound healing. *Nagoya J Med Sci*. 2018;80(2):141–153. doi:10.18999/nagjms.80.2.141.
22 Stump A, Bedri M, Goldberg NH, Slezak S, Silverman RP. Omental transposition flap for sternal wound reconstruction in diabetic patients. *Ann Plast Surg*. 2010;65(2):206–210. doi:10.1097/SAP.0b013e3181c9c31a.
23 Mazzaferro D, Song P, Massand S, Mirmanesh M, Jaiswal R, Pu LLQ. The Omental Free Flap—A Review of Usage and Physiology. *J Reconstr Microsurg*. 2018;34(3):151–169. doi:10.1055/s-0037-1608008.
24 De Siena R, Balducci L, Blasi A, et al. Omentum-derived stromal cells improve myocardial regeneration in pig post-infarcted heart through a potent paracrine mechanism. *Exp Cell Res*. 2010;316(11):1804–1815. doi:10.1016/j.yexcr.2010.02.009.
25 Bahamondes F, Flores E, Cattaneo G, Bruna F, Conget P. Omental adipose tissue is a more suitable source of canine Mesenchymal stem cells. *BMC Vet Res*. 2017;13(1):166. doi:10.1186/s12917-017-1053-0.
26 Singh AK, Pancholi N, Patel J, et al. Omentum facilitates liver regeneration. *World J Gastroenterol*. 2009;15(9):1057–1064. doi:10.3748/wjg.15.1057.
27 Zhang J, Guan J, Niu X, et al. Exosomes released from human induced pluripotent stem cells-derived MSCs facilitate cutaneous wound healing by promoting collagen synthesis and angiogenesis. *J Transl Med*. 2015;13:49. doi:10.1186/s12967-015-0417-0.
28 Memmert S, Nokhbehsaim M, Damanaki A, et al. Role of cathepsin S In periodontal wound healing-an in vitro study on human PDL cells. *BMC Oral Health*. 2018;18(1):60. doi:10.1186/s12903-018-0518-2.
29 Flynn CM, Garbers Y, Düsterhöft S, et al. Cathepsin S provokes interleukin-6 (IL-6) trans-signaling through cleavage of the IL-6 receptor in vitro. *Sci Rep*. 2020;10(1):21612. doi:10.1038/s41598-020-77884-4.
30 Shi GP, Sukhova GK, Kuzuya M, et al. Deficiency of the cysteine protease cathepsin S impairs microvessel growth. *Circ Res*. 2003;92(5):493–500. doi:10.1161/01.RES.0000060485.20318.96.
31 Iorio V, Troughton LD, Hamill KJ. Laminins: Roles and Utility in Wound Repair. *Adv Wound Care (New Rochelle)*. 2015;4(4):250–263. doi:10.1089/wound.2014.0533.
32 Swerts JP, Soula C, Sagot Y, et al. Hemopexin is synthesized in peripheral nerves but not in central nervous system and accumulates after axotomy. *J Biol Chem*. 1992;267(15):10596–10600. doi:10.1016/S0021-9528(19)50058-8.
33 Zhu Y, Qiu Y, Chen M, et al. Hemopexin is required for adult neurogenesis in the subventricular zone/olfactory bulb pathway. *Cell Death Dis*. 2018;9(3):268. doi:10.1038/s41419-018-0328-0.

34 Dong B, Zhang Z, Xie K, et al. Hemopexin promotes angiogenesis via up-regulating HO-1 in rats after cerebral ischemia-reperfusion injury. *BMC Anesthesiol*. 2018;18(1):2. doi:10.1186/s12871-017-0466-4.

35 Siriwach R, Ngo AQ, Higuchi M, et al. Single-cell RNA sequencing identifies a migratory keratinocyte subpopulation expressing THBS1 in epidermal wound healing. *iScience*. 2022;25(4):104130. doi:10.1016/j.isci.2022.104130.

36 Ashcroft GS, Kielty CM, Horan MA, Ferguson MW. Age-related changes in the temporal and spatial distributions of fibrillin and elastin mRNAs and proteins in acute cutaneous wounds of healthy humans. *J Pathol*. 1997;183(1):80–89. doi:10.1002/(SICI)1096-9896(199709)183:1<80::AID-PATH1104>3.0.CO;2-N.

37 Handa K, Abe S, Suresh VV, et al. Fibrillin-1 insufficiency alters periodontal wound healing failure in a mouse model of Marfan syndrome. *Arch Oral Biol*. 2018;90:53–60. doi:10.1016/j.archoralbio.2018.02.017.

38 Zuliani-Alvarez L, Midwood KS. Fibrinogen-Related Proteins in Tissue Repair: How a Unique Domain with a Common Structure Controls Diverse Aspects of Wound Healing. *Adv Wound Care (New Rochelle)*. 2015;4(5):273–285. doi:10.1089/wound.2014.0599.

39 Farrell DH. Pathophysiologic roles of the fibrinogen gamma chain. *Curr Opin Hematol*. 2004;11(3):151–155. doi:10.1097/01.moh.0000131440.02397.a4.

40 Juhasz I, Murphy GF, Yan HC, Herlyn M, Albelda SM. Regulation of extracellular matrix proteins and integrin cell substratum adhesion receptors on epithelium during cutaneous human wound healing in vivo. *Am J Pathol*. 1993;143(5):1458–1469.

41 Schneider H, Mühle C, Pacho F. Biological function of laminin-5 and pathogenic impact of its deficiency. *Eur J Cell Biol*. 2007;86(11–12):701–717. doi:10.1016/j.ejcb.2006.07.004.

42 Sinno H, Malholtra M, Lutfy J, et al. Topical application of complement C3 in collagen formulation increases early wound healing. *J Dermatolog Treat*. 2013;24(2):141–147. doi:10.3109/09546634.2011.631977.

43 Lenselink EA. Role of fibronectin in normal wound healing. *Int Wound J*. 2015;12(3):313–316. doi:10.1111/iwj.12109.

44 Tonnesen MG, Feng X, Clark RA. Angiogenesis in wound healing. *J Investig Dermatol Symp Proc*. 2000;5(1):40–46. doi:10.1046/j.1087-0024.2000.00014.x.

45 Nikoloudaki G, Creber K, Hamilton DW. Wound healing and fibrosis: a contrasting role for periostin in skin and the oral mucosa. *Am J Physiol Cell Physiol*. 2020;318(6):C1065-C1077. doi:10.1152/ajpcell.00035.2020.

46 Yin SL, Qin ZL, Yang X. Role of periostin in skin wound healing and pathologic scar formation. *Chin Med J (Engl)*. 2020;133(18):2236–2238. doi:10.1097/CM9.0000000000000949.

47 Argüeso P, Mauris J, Uchino Y. Galectin-3 as a regulator of the epithelial junction: Implications to wound repair and cancer. *Tissue Barriers*. 2015;3(3):e1026505. doi:10.1080/21688370.2015.1026505.

48 Takaku S, Niimi N, Kadoya T, et al. Galectin-1 and galectin-3 as key molecules for peripheral nerve degeneration and regeneration. *AIMS Mol Sci*. 2016;3(3):325–337. doi:10/3934/molsci.2016.3.325.

49 McLeod K, Walker JT, Hamilton DW. Galectin-3 regulation of wound healing and fibrotic processes: insights for chronic skin wound therapeutics. *J Cell Commun Signal*. 2018;12(1):281–287. doi:10.1007/s12079-018-0453-7.

50 Pastar I, Stojadinovic O, Yin NC, et al. Epithelialization in Wound Healing: A Comprehensive Review. *Adv Wound Care (New Rochelle)*. 2014;3(7):445–464. doi:10.1089/wound.2013.0473.

51 Klasan GS, Ivanac D, Erzen DJ, et al. Reg3G gene expression in regenerating skeletal muscle and corresponding nerve. *Muscle Nerve*. 2014;49(1):61–68. doi:10.1002/mus.23877.

52 Hennebry SC, Eikelis N, Socratous F, Desir G, Lambert G, Schlaich M. Renalase, a novel soluble FAD-dependent protein, is synthesized in the brain and peripheral nerves. *Mol Psychiatry*. 2010;15(3):234–236. doi:10.1038/mp.2009.74.

53 Barrett PM, Topol EJ. The fibrillin-1 gene: unlocking new therapeutic pathways in cardiovascular disease. *Heart*. 2013;99(2):83–90. doi:10.1136/heartjnl-2012-301840.

54 Sabatino M, Kim-Schulze S, Panelli MC, et al. Serum vascular endothelial growth factor and fibronectin predict clinical response to high-dose interleukin-2 therapy. *J Clin Oncol*. 2009;27(16):2645–2652. doi:10.1200/JCO.2008.19.1106.

55 Fu H. *Interleukin 35 Inhibits Ischemia-Induced Angiogenesis Essentially through the Key Receptor Subunit Interleukin 12 Receptor Beta 2*. Dissertation. Temple University; 2019. doi:10.34944/dspace/519.

56 Chamorro M, Carceller F, Llanos C, Rodríguez-Alvariño A, Colmenero C, Burgueño M. The effect of omental wrapping on nerve graft regeneration. *Br J Plast Surg*. 1993;46(5):426–429. doi:10.1016/0007-1226(93)90050-L.